Improvement to the Range Stack Straw Chamber Electronics

Xinghua Li, Douglas Bryman, Toshio Numao,
Miles Constable, John Cresswell, Ray Bula

TRIUMF
4004 Wesbrook Mall
Vancouver, BC
Canada V6T 2A3

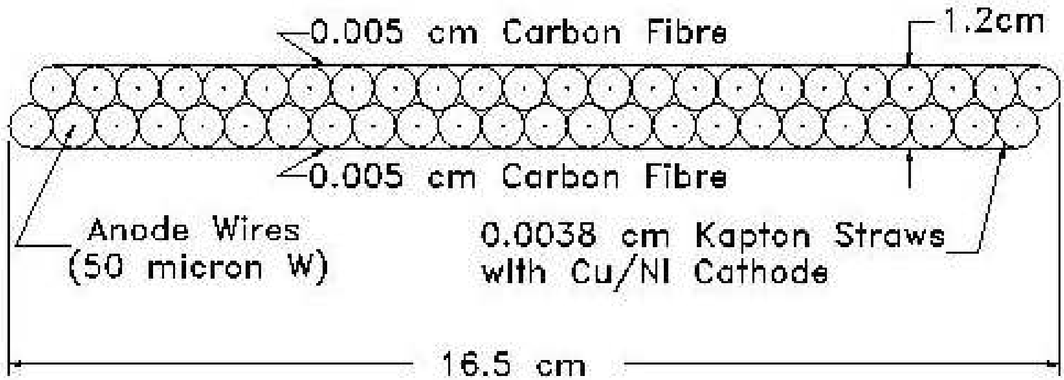

Figure 1: *End view of an inner RSSC.*

1 Introduction

The E787/949 RSSCs are intended to give a precise measurements of tracking information of particles traversing or stopping in the range stack. There was a long-standing problem of poor resolution in the RSSC longitudinal (z) measurement. This report focuses on understanding the source of the problem and provides a technique for improving the performance.

2 Range Stack Straw Chamber

2.1 RSSC geometry

The E787/E949 RSSCs were built in Princeton University. They are located after layer 10 and layer 14 of the Range Stack (RS). The inner RSSC consists of 2 sublayers of 24 straw tubes per sector (see Fig. 1) and the outer RSSC consists of 2 sublayers of 28 straws per sector. The mass per cm^2 is $0.054g/cm^2$. Each straw tube is 3.4 mm in radius and has a 38-μm thick Kapton-coated Cu/Ni cathode and 50-μm diameter gold-coated tungsten anode wire. The two sublayers of straw tubes are offset by one half cell from each other so that high efficiency can be guaranteed. A detailed drawing is given in Figure 1. The x-axis of a chamber is defined to be along the width of the chamber. There are a total of 48 chambers, with 2496 straws currently installed in the E949 experiment.

Two straws in the same sublayer are connected in pairs on the upstream end by using a dedicated "jumper card" (The top part in Fig. 2). Connected straws are separated by 12 (14) straws, for the inner (outer) chambers, reducing the electronic channel count from 2496 straws to 1248 pairs. The chambers are read out from only the downstream end because of the severe space constraints and the desire to have the smallest possible cable length between the chambers and the external readout. Figure 2 shows a top view of the RSSC.

The advantages of this design are:

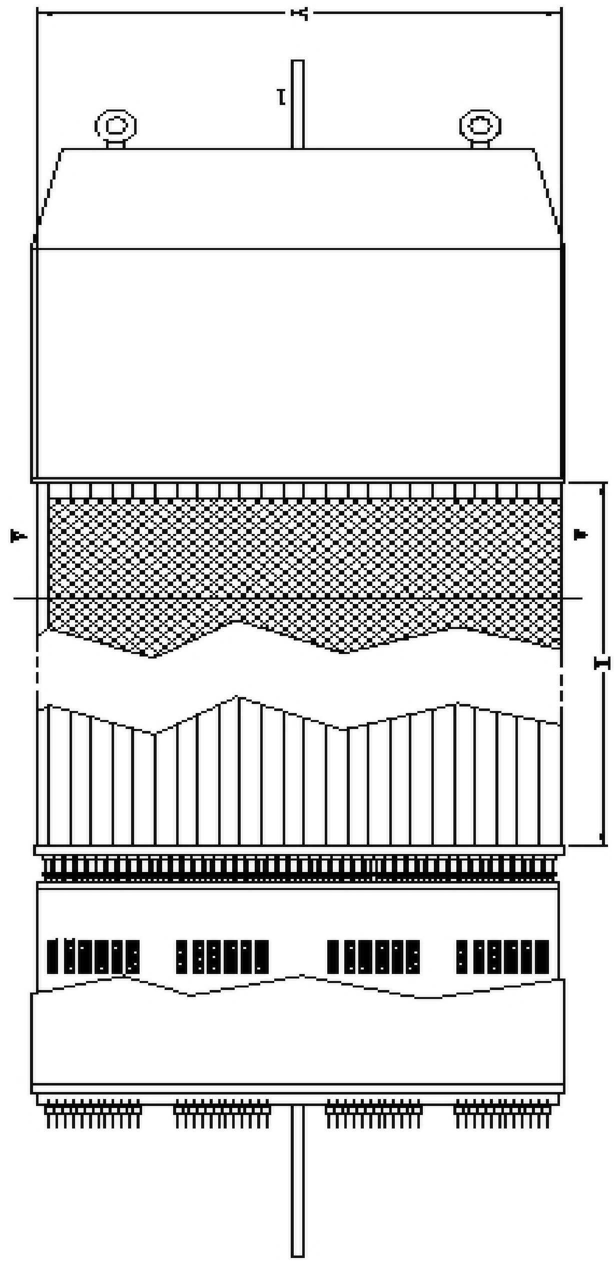

Figure 2: *Top view of an inner RSSC. Connected straws are separated by 12 straws. The "jumper card" is on the top part of this figure.*

- The cells are isolated from each other by the cathode. Therefore, cross talk between cells along the wire is minimized.
- The structure of the straw chamber allows unambiguous localization in xy plane.
- The resolution of tracks is independent of a particle's incident angle in the xy plane, so one does not have to incorporate angular correction factors.

2.2 RSSC readout electronics

The description in this section is obtained from reference[9]. The E787 RSSC read out scheme is sketched in Figure 3 for one pair of straw tubes. Since an access to the chambers is very difficult, no active electronics components are mounted on the chambers (see Fig. 3 a) for Chamber Front End). There are no pre-amplifiers on the chambers since the RSSC works on the limited streamer mode. The analog signals are transmitted from the chambers through coaxial cables to the external electronics (see Fig. 3 b) Chamber Readout Card).

In Fig. 3 a) part, the front end consists of a 2-layer readout-card, with a daughter board containing a set of sockets that line up with pins connected to the chamber wires that plug into the end of the chamber. This card takes up minimal space, and is part of the mechanical structure of the chamber itself. The straw walls are held at signal ground through a conductive-epoxy connection from the straws to an aluminum gas tight end-piece box, which is mechanically connected to the readout-card with small brass bolts. The high voltage is distributed onto a bus on the front-end card, and to each straw pair through a 10 MΩ surface-mount resistor. The signals pass through a surface-mount HV blocking capacitor, a resistor to match the straw impedance to the cables, and then through a connector built into the chamber to the cables themselves. The key elements in the front end are the custom surface mount resistors and capacitors used for HV distribution and blocking. While the resistors do not typically hold significant voltage, this custom thick-film elongated surface mount part is able to withstand HV sparks.

The b) part of the Fig. 3 shows the chamber readout electronics - Princeton board. There are 28 channels per board, which reads out either one inner or one outer chamber. The first active electronics the signals see is a Lecroy MVL407 comparator. After forcing one end of the pair to always come late using a 25 nsec passive delay line, a time difference pulse is formed using a 10H131 ECL flip-flop. Note that the flip-flop clock is disabled while the primary time-difference pulse is being formed, so that the channel is disabled while the time stretcher is active, and the channel is self-reseting if no "late" pulse arrives. The primary time difference pulse is about 25 ± 7 nsec wide, with the z measurement encoded in that pulse width. This pulse is stretched by about a factor of 45 using a linear "Time Stretcher" circuit, making it about 1100 ± 300 nsec. With a modest 1 nsec resolution on the stretched pulse width, 20 psec resolution on the primary pulse width is obtained, which would be a 0.3 cm resolution z measurement. In practice, when running the chambers in the experiment, a 1 cm z resolution can be achieved. The linear time stretcher circuit is schemed in Fig 4. The complete readout system underwent a fairly severe set of tests done by the Princeton group: linearity, temperature variation, power supply voltage variations and magnetic field effects. The test results are listed in table 1.

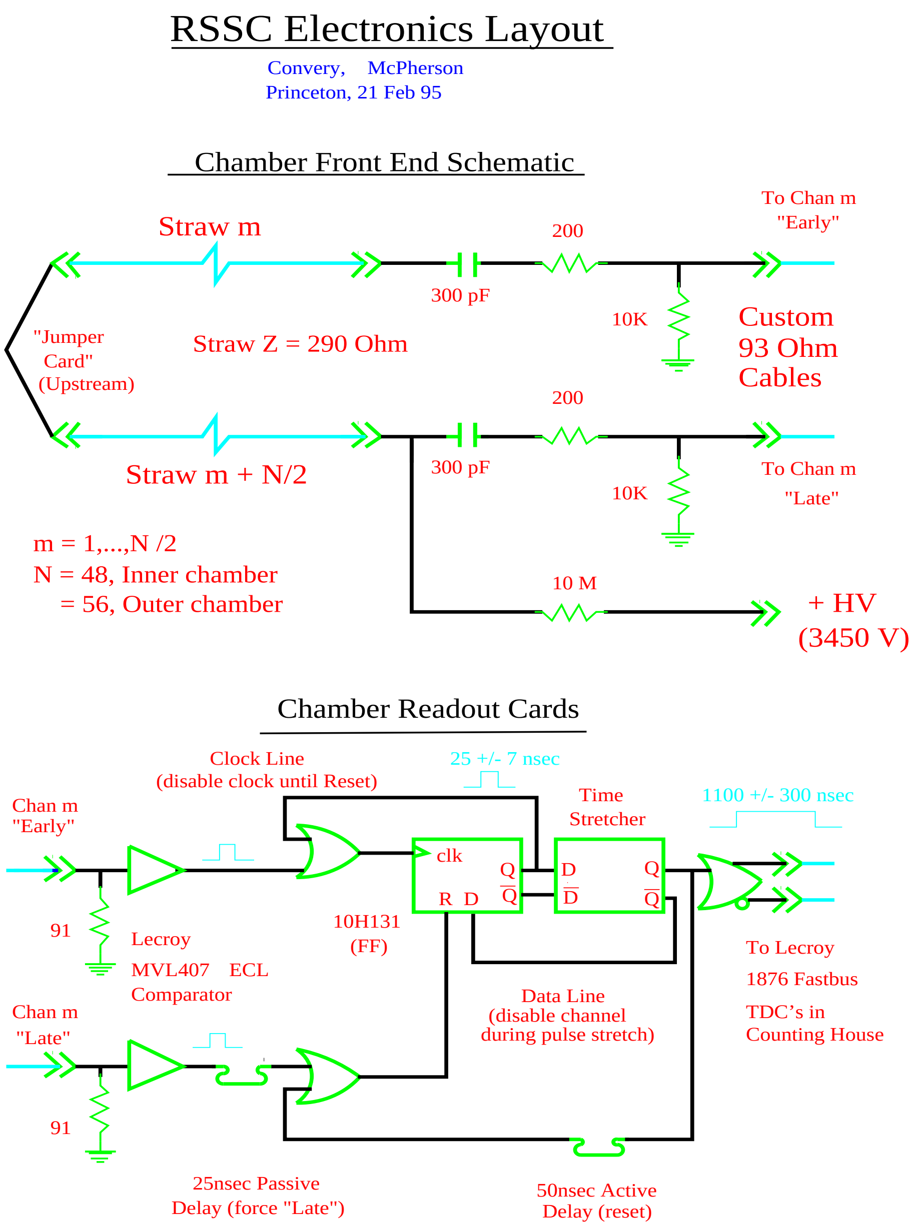

Figure 3: *The RSSC electronics readout[9]. The top a) is the front end electronics. The bottom b) is the external electronics.*

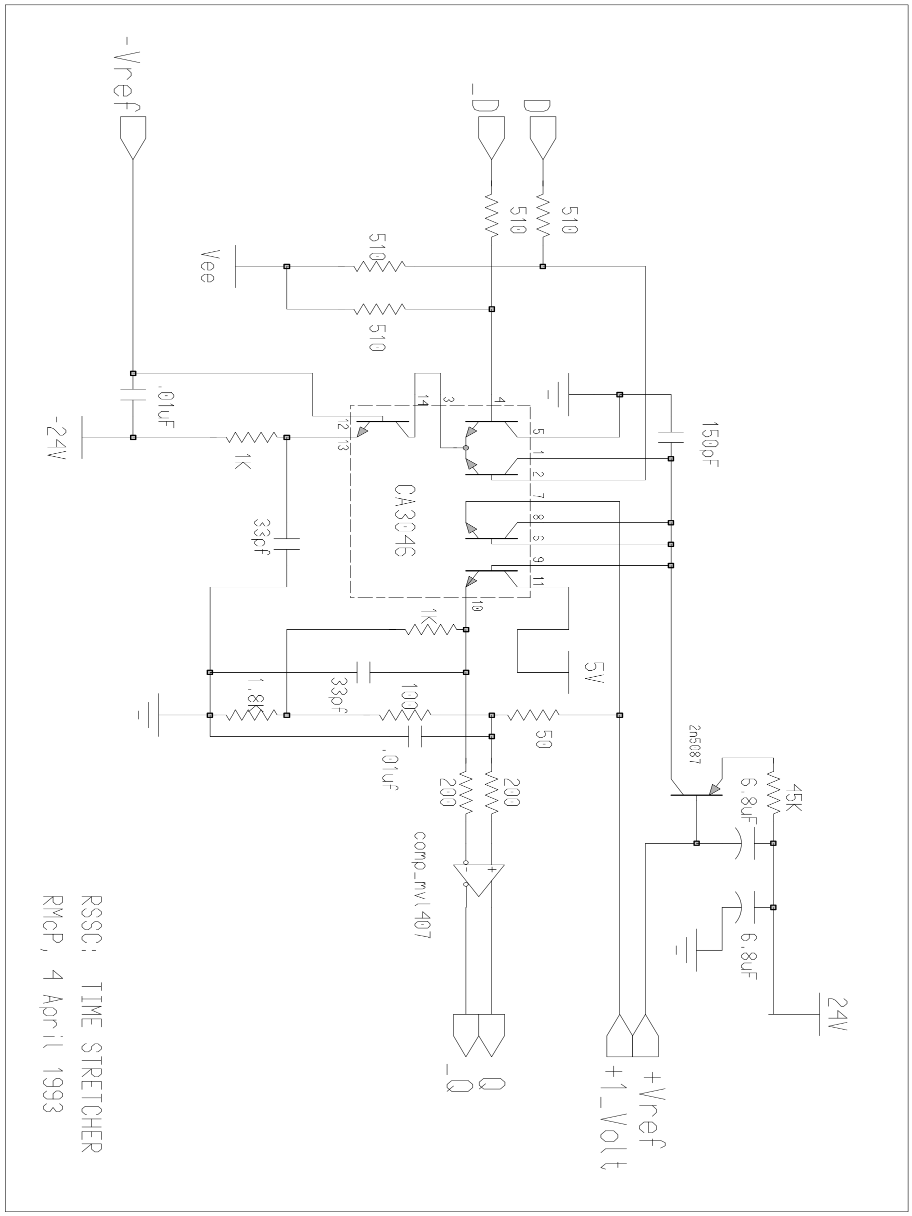

Figure 4: *The time stretcher schematic. The design is adapted from a Lecroy time-of-flight TDC. "Vref" is about 9 volts[9].*

Description	Results
Linearity	Typical Deviations from linear fit of ± 20 psec primary pulse width, over a range of 15-35 nsec widths
Temperature Variation	Better than ± 2 psec per degree Celsius primary pulse width, 5-35 degree Celsius
Power Supply Variation	-2 V supply: 1.5 psec per mV, primary pulse width -5.2 V supply: 0.2 psec per mV, primary pulse width rest: negligible
Magnetic Fields	No observable effects in fields up to 200 Gauss. (Stray field at electronics racks < 20 Gauss)

Table 1: *Tests performed end-to-end time readout circuit[9].*

2.3 Limited streamer mode theory

The theoretical description in this section is reproduced from references[1],[2],[3] and [4]. The straw chambers are operated in limited streamer mode. The model for streamer formation is based on Townsend gas discharge theory and space charge effects which distort the electric field near the anode wire and limit the electron avalanche[1]. The streamer nature of the discharge was established by Charpak et al.[2] and Fisher et al.[3]. It was observed that the centroid of charge generated by the process was definitely away from the center of the wire, suggesting a propagation from the wire towards the cathode.

Figure 5[5] gives a traditional picture of the streamer mode – the relationship between the high voltage and the gain of working in the proportional state and in the streamer state. At low voltage, the behavior is characterized by an exponential dependence on the high voltage. This is the proportional mode. At the high voltage end of the scale, there is a sudden transition to a mode of operation, where the charge collected on the anode is a linear function of the voltage. The output charge in this mode is less dependent of the initial ionization. This is the so-called limited streamer mode. Also indicated are two advantages for the limited streamer mode over the proportional mode. One is higher gain (up to 10^8) than that of proportional mode, the other is the collected charge is less sensitive to high voltage fluctuations.

The avalanche process is depicted in Fig. 6. The particle passes through the chamber and a cluster of ionization electrons is formed. The electron and ion mobilities differ by a factor of about 10^3. Thus, the electrons are collected on the anode wire in a few tens of nanoseconds, whereas the positive ions are essentially stationary during this collection time, creating space charge. The avalanche process follows the usual exponential behavior in the proportional region in Fig.5. The rate of growth of the avalanche slows down as the voltage exceeds a certain value indicating that space charge saturation is felt by

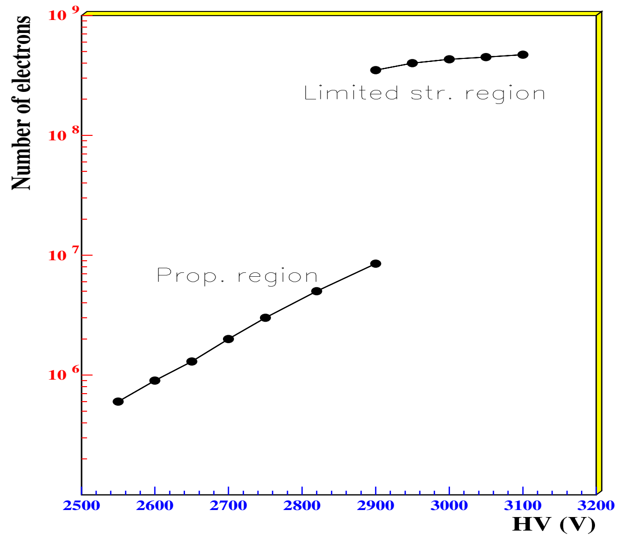

Figure 5: *Collected charge as a function of voltage (a 100μm diameter wire in a tube* 12×12*, filled with* $Ar(49.3\%)+C_2H_6(49.3\%)+CH_3CH_2OH(1.4\%)$*).*

the multiplying electrons, and cancels the applied electric field[6]. As a result, radiative recombination may occur. For instance, for a gas mixture Argon and isobutane, the process of recombination goes by the following two reactions[4]:

$$A^+ + e^- \rightarrow A^* + \gamma \tag{1}$$

The energy of the emitted photons could be high enough to reach outside of the space charge cloud and produce electrons there from ionizing isobutane molecules[1] by the process:

$$\gamma + C_4H_{10} \rightarrow C_4H_{10}^+ + e^-. \tag{2}$$

These emitted electrons drift to the anode wire giving rise to the observed current signal.

The streamers quench themselves in a well controlled way providing uniform electronic pulses for a given energy loss from a traversing particle. Once the streamer process is triggered by the recombination photons, it will continue until the last such photon creates an electron at the streamer front. This streamer process is depicted in Fig.7

In short, in an iterative sequence, the amplification process develops towards the cathode and extinguishes itself with the proper gas mixture. Hence, the limited streamer mechanism is a consequence of a delicate balance of the electron avalanche in an electric field, which is dynamically adjusted by the avalanche process itself.

[1]Isobutane here serves as a quenching gas.

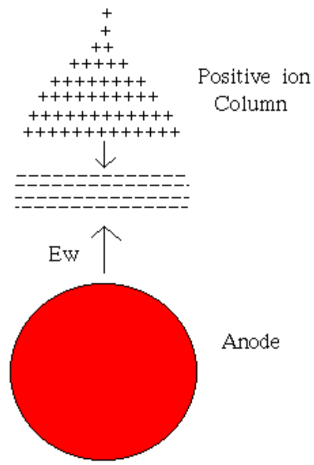

Figure 6: *Schematic diagram of the avalanche process.*

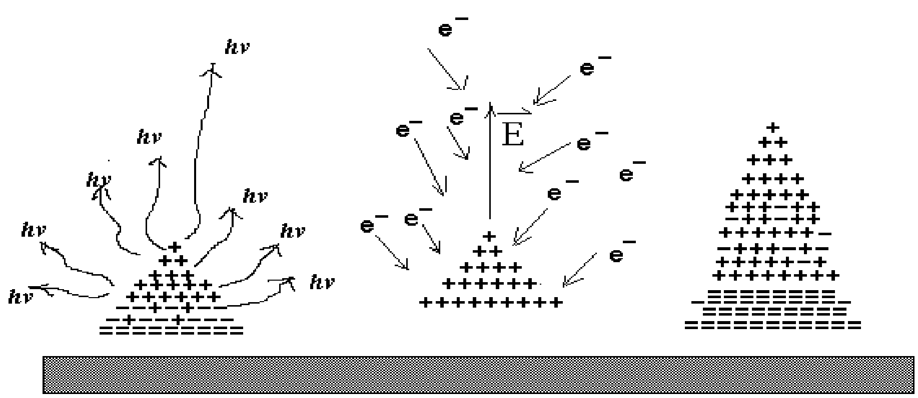

Figure 7: *Schematic description of the self quenching streamer phenomena.*

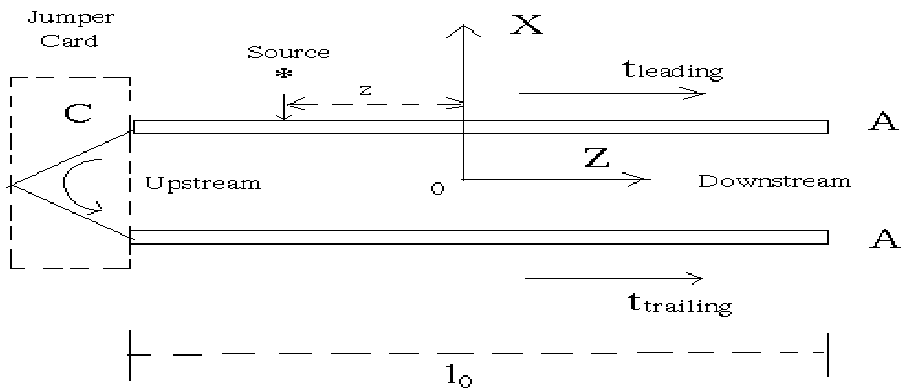

Figure 8: *Schematic diagram of the end-to-end time method.*

2.4 End-to-end timing method

RSSCs use the end-to-end timing to get z information. the idea is shown in Fig. 8. The origin in RSSC is defined just in the middle of the RSSC. When a particle hits a tube, signals travel to the downstream and the upstream ends, respectively. Since both signals are read out from the downstream end, one of them always travels a longer distance than the other and takes longer traveling time. The earlier signal is called the leading edge time signal and the later one is called the trailing edge time signal. Their time difference is proportional to the hit z position for a given constant propagation speed in each tube. Suppose the whole tube length is l_0, the velocity is v_0, the signal travel distance in the jumper card is c_0, $t_{leading}$ is the leading edge signal time and $t_{trailing}$ is the trailing edge signal time, corresponding to the signals from end A and end A' respectively. The hit position z can be figured out using the following equations:

$$v_0 t_{trailing} = l_0 + (\frac{l_0}{2} + z) + c_0 \tag{3}$$

$$v_0 t_{leading} = (\frac{l_0}{2} - z) \tag{4}$$

from the above two equations:

$$v_0(t_{trailing} - t_{leading}) = l_0 + 2z + c_0 \tag{5}$$

Thus:

$$z = \frac{v_0 \Delta t - (l_0 + c_0)}{2} \tag{6}$$

where $\Delta t = t_{trailing}$ - $t_{leading}$

	σ_z(M.C.) (cm)	σ_z(Data) (cm)	$\Delta\sigma_z$ (cm)
Inner upstream	1.37	2.88	2.53
Inner downstream	1.33	3.21	2.92
Outer upstream	2.12	2.79	1.81
Outer downstream	2.09	2.97	2.11

Table 2: *Residual (Z_{UTC} - Z_{RSSC}) resolution of the $K_{\pi 2}$ from the Monte Carlo simulation and from a 1998 data. Upstream is defined as $z < 0$, while downstream is defined as $z > 0$. $\Delta\sigma_z$ is the difference of the z resolution between the first two columns.*

3 Problem and resolution

3.1 Study of pion samples

The residual (Z_{UTC} - Z_{RSSC}) resolutions of $K_{\pi 2}$[2] from the Monte Carlo simulation and from a 1998 data sample were studied to unfold what is behind the poor resolution.

The distributions of the residual are plotted in Fig. 9. The resolutions of the residual are listed in Table 2.

The worse observed resolutions indicate that there are contributions, other than physics contributions[3], to the z measurements, which can be represented by the differences[4] between the MC and the data in the last column of Table 2. From this column, the downstream ends show worse resolutions than those on the upstream ends. The RSSC electronics contributions on the upstream and downstream ends should be identical, considering the fact that the upstream and the downstream share the same electronics channel. The worse results on the downstream ends indicate that the contributions include an unknown source, other than the RSSC electronics contribution. And the unknown contribution has a larger impact on the downstream ends. Also, in this column, better resolutions can be obtained in the outer RSSCs. However, in the MC, the outer RSSCs show worse resolutions due to greater multiple scattering. And the electronics contributions from the inner and outer RSSCs should be identical due to the similar electronics. The better performance in the outer RSSCs indicate the unknown contribution overrides the physics contributions and has a smaller impact on the outer RSSCs. Explanations will be given in section 3.3.

[2]For the $K_{\pi 2}$ sample, events are required not to be a beam background, have photon detected and be well reconstructed and identified not to be muons with momentum < 211 MeV/c, Range < 33 cm and energy < 115 MeV.

[3]Physics contributions to the z resolution include the π^+-nuclear interaction and multiple scattering effects in the range stack, which can be simulated by the Monte Carlo simulation.

[4]
$$\Delta\sigma_z = \sqrt{\sigma_{data}^2 - \sigma_{umc}^2}. \tag{7}$$

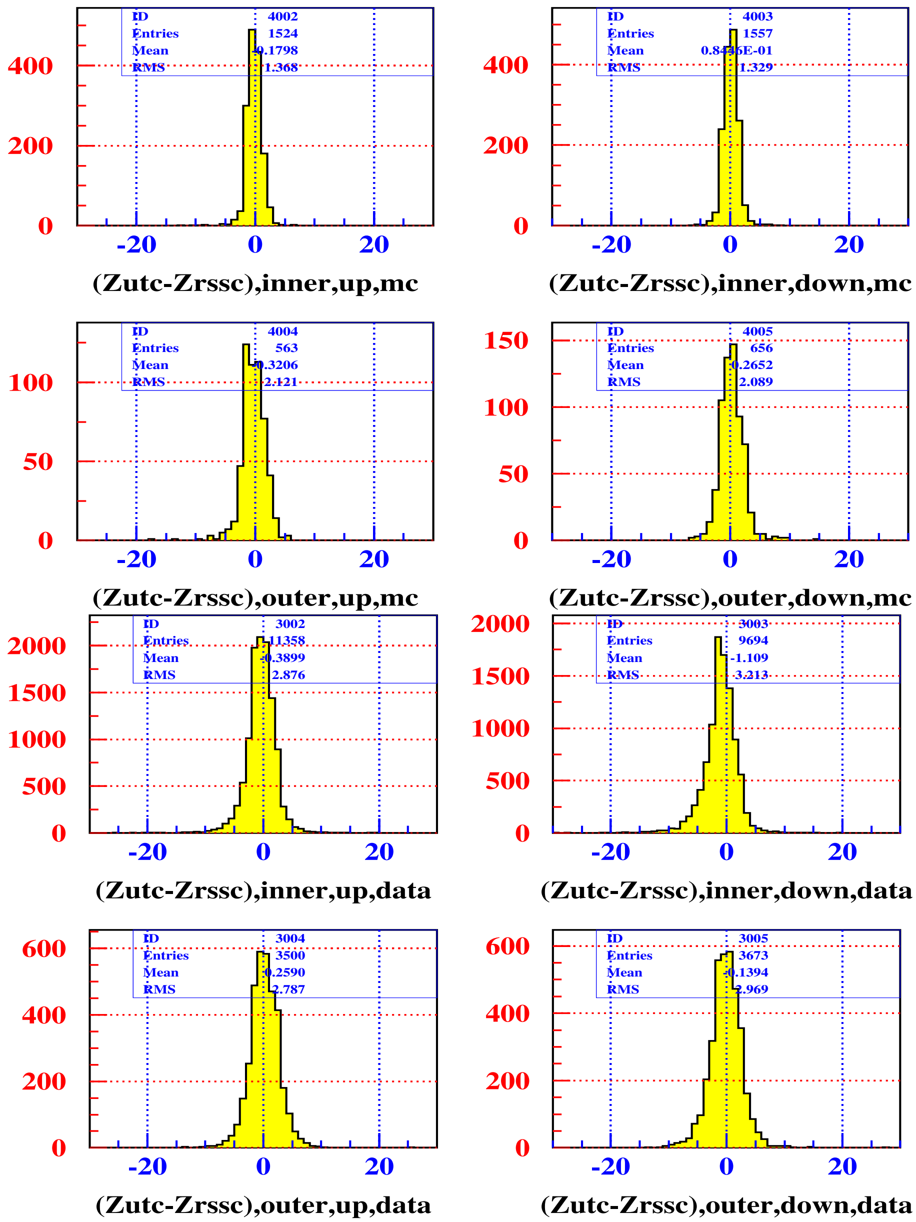

Figure 9: *Residual (Z_{UTC} - Z_{RSSC}) of the $K_{\pi 2}$ sample from the Monte Carlo simulation and the 1998 data. 'Inner' indicates the inner RSSC; 'outer' indicates the outer RSSC; 'up' indicates the upstream end; 'down' indicates the downstream end; 'mc' indicates the Monte Carlo simulation; 'data' indicates the 1998 data.*

position	resolution from an ^{55}Fe source			resolution from a ^{106}Ru source		
z (cm)	W_1	W_2	W_3 (cm)	W_1	W_2	W_3 (cm)
36	0.94	1.21	0.94	3.81	5.90	4.61
2.0	0.64	0.95	0.75	2.59	2.70	3.00
-34	0.70	1.17	0.81	2.64	2.15	2.35

Table 3: *Z resolution comparison from an ^{55}Fe source and a ^{106}Ru source for an inner RSSC. The former resolution was better than the latter's due to the larger amplitude. W_1 indicates tube 1. W_2 indicates tube 2. W_3 indicates tube 3.*

3.2 Further study about contributions to the resolution

It is hypothesized that the unknown contribution to the RSSC z resolution depends on pulse amplitude. The larger the amplitudes are, the better the resolutions are.

Bench tests were done using an ^{55}Fe source[5] and a well-collimated ^{106}Ru source[6] to confirm this hypothesis. Sources were put on the tube 1, tube 2 and tube 3 of the RSSC on the downstream, middle and upstream positions, respectively. The z measurement resolutions, listed in Table 3, show the results from the ^{55}Fe source was better than that from the ^{106}Ru source due to the fact that the signal amplitudes of the former are much larger than the latter's.

3.3 Time-walk effect

Based on the image from the true pulses shown in Fig. 10, an explanation to the poor z resolution may be given - the resolution depends on the signal amplitudes due to time walk. The pulse images, in Fig. 10, show the leading edge timings from two adjacent channels shifting because of the different amplitudes.

Consider, for example, two signals of different pulse height but exactly coincident in time as shown in Fig. 11. Suppose these signals are introduced into a discriminator with a fixed threshold. Because of the difference in amplitude, signal A will trigger at time t_a and signal B will trigger at t_b, although both are exactly coincident. The dependence on amplitude causes the logic signal to "walk". This phenomenon contributes to the poor RSSC z resolution. Then, we can answer the questions left in section 3.1. For the downstream end, the worse resolution is due to the greater attenuation and dispersion of the signals. When a hit occurs on the downstream end, the attenuation difference from both ends is larger than that when a hit occurs on the upstream end. Hence, larger time walk occurs when hits are on the downstream end leading to the worse z measurements. Also, the better resolutions in the outer RSSCs is because the smaller

[5]For the ^{55}Fe source, only one tube is hit per event. ^{55}Fe decays via electron capture to ^{55}Mn, which de-excites and produces a 6 keV K x-ray. If the x-ray is captured in the chamber gas, a localized ionization avalanche is created, resulting in a pulse resembling one from a charged track in the straw.

[6]As for the ^{106}Ru source, the situation is similar to the E787/E949 circumstance since the ^{106}Ru emits electrons which pass through the chamber and create limited streamers in the chamber gas.

Figure 10: *Typical RSSC pulses from two adjacent straws. Different amplitudes result in time shift due to the fixed discriminator threshold. The bottom two curves are the part between two vertical dashed lines in the falling edges of the top two curves, which are enlarged to show the time shift clearly.*

traversing velocities (the larger energy losses) in the outer RSSCs than in the inner, giving larger pulse amplitudes and leading to smaller time walk.

3.4 Cross talk

When a particle hits a tube, a smaller amplitude cross talk can be induced in neighbor tubes. Each straw tube is isolated from the others by a metal isolating film, minimizing the possible cross talk along the tube. However, the connection of the straw pairs on the upstream end and the connection between the chamber and the external cables have little shielding protection. Cross talk can occur at any of the three positions (A, A', C) indicated in Figure 8. For the E787 RSSC system, cross talk is negligible since it is suppressed by a high discriminator threshold.

3.5 Add-on board

From section 3.3, one can conclude: the larger the signal amplitudes are, the smaller time walk is. Thus, if we can increase the signal amplitude, better z measurement can be achieved. One possible solution is to increase the high voltage. The E787 RSSCs system would work well if we could increase the voltage gain. The higher gain means more ionizated electrons collected on the anode wire per event, giving a larger pulse amplitude. However, this approach is infeasible due to the RSSC breakdown at higher voltage.

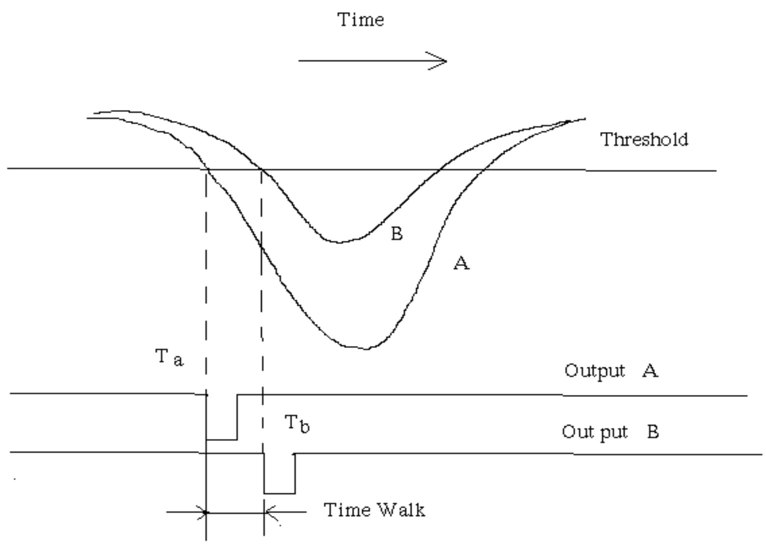

Figure 11: *Schematic diagram of the time walk effect.*

The other possible solution is to add an amplifier. However, when adding an amplifier, cross talk amplitudes may increase proportionally and may pass the discriminator threshold.

In order to get around this shortcoming, we designed a new dual-discriminator add-on board to go between the chamber and the existing external electronics - Princeton board. A high threshold eliminates cross talk and a low threshold is used to minimize time walk. The add-on board has 56 channels . Each channel includes: two amplifiers, a high-threshold discriminator, a low-threshold discriminator a delay line and a coincidence. Fig. 12 shows the circuit diagram for an add-on board channel.

Signals coming from the RSSC are fed into the two amplifiers. Then, the analog signal is divided into two identical parts: one goes into the high threshold discriminator; the other one goes into the low threshold discriminator. The logical signal from the low threshold discriminator is delayed about 5 ns before being fed into a coincidence. Fig. 13 shows how the two-discriminator system works. Since the logical signal from the low threshold discriminator is delayed, the low threshold actually determines the start time of the signal. The high threshold serves to remove cross talk pulses.

3.6 Thresholds

Normally, the low discriminator threshold is set just above the noise level. In order to determine a suitable high discriminator threshold value to suppress cross talk, bench tests using a ^{106}Ru shown in Fig. 14 and an ^{55}Fe[7] sources were done and results are shown in Fig. 15. The cross talk count rate, e.g. for the ^{106}Ru source, is described using the

[7]The basic setup is the same as with the ^{106}Ru source, except there is no scintillator trigger.

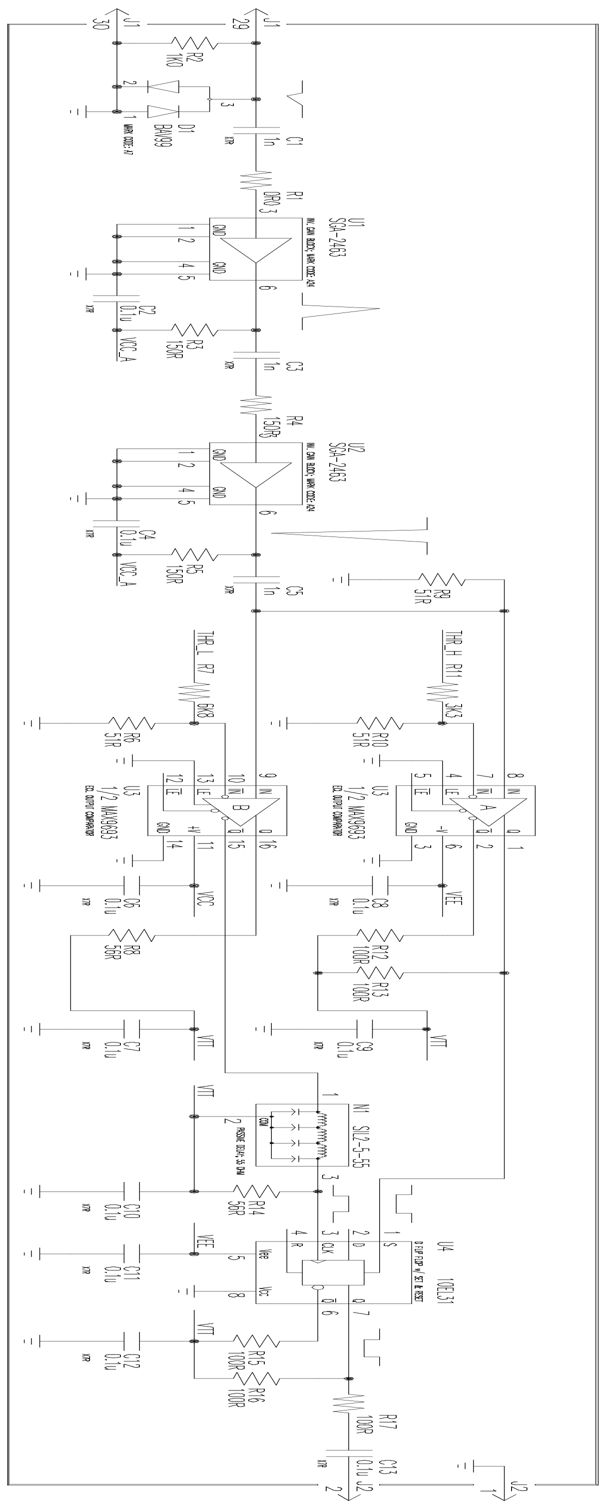

Figure 12: *Circuit diagram for a typical add-on board channel. Signals are fed from the top to the bottom.*

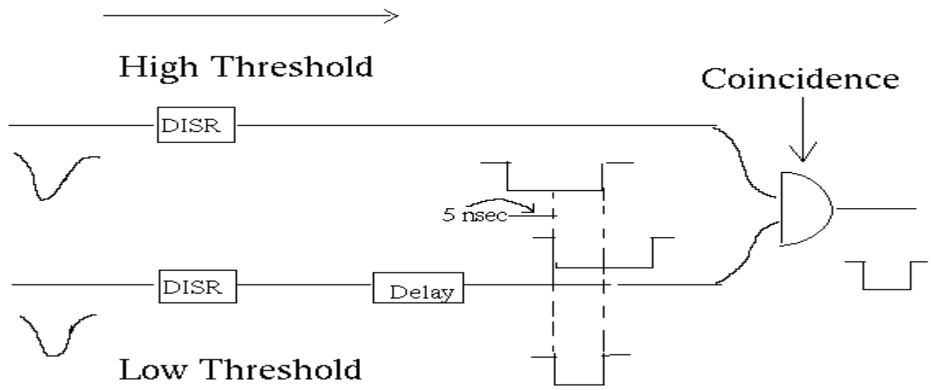

Figure 13: *The logic diagram of the dual thresholds of the new electronics.*

scintillator and the ith tube as a trigger to investigate the cross talk in neighbor tube[8].

The left graph in Fig. 15 is for the ^{106}Ru source. The source was put on the ith tube. Most of cross talk was removed when the high thresholds were set at > 60 mV. The circles show cross talk induced into a neighbor tube laying in a different sublayer of the RSSC. The rate did not drop down to zero since a particle usually hits two adjacent tubes in different sublayers simultaneously. The triangles show cross talk in a neighbor tube in the same sublayer of the RSSC. The rate was almost down to zero above 60 mV since a particle can't hit two adjacent tubes in the same sublayer simultaneously.

The right graph in Fig. 15 was obtained using the ^{55}Fe source to observe the pure cross talk effect. For the ^{55}Fe source, only one tube is hit per event. Thus, when measuring cross talk rate by using an adjacent tube as a trigger, only cross talk induced from that trigger wire is present. When the high threshold was above 60 mV, almost all of the cross talk was removed. Thus, the rate shown in the right graph went down to zero above 60 mV.

It appears that a 60 mV high threshold is suitable to suppress cross talk for all cases.

---

[8]

$$Rate = (W_i \cdot Scin \cdot W_{i+1})/(Scin \cdot W_i). \tag{8}$$

where 'W_i' and '$W(i+1)$' represents the hits on tube i and tube (i+1) respectively, and 'Scin' represents the hits on the scintillator.

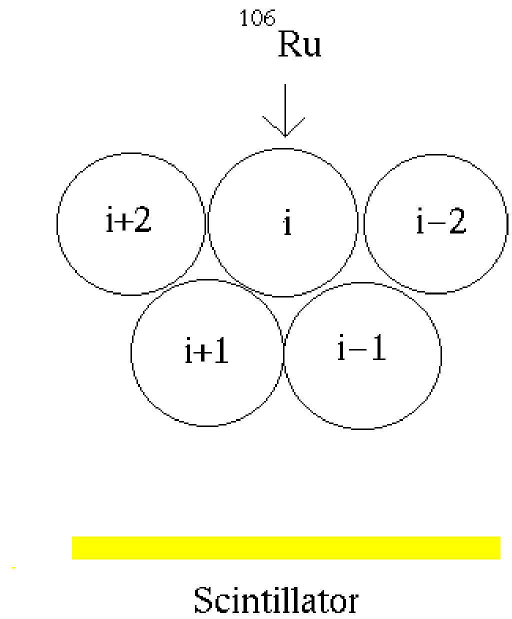

Figure 14: *The experiment setup for bench test.*

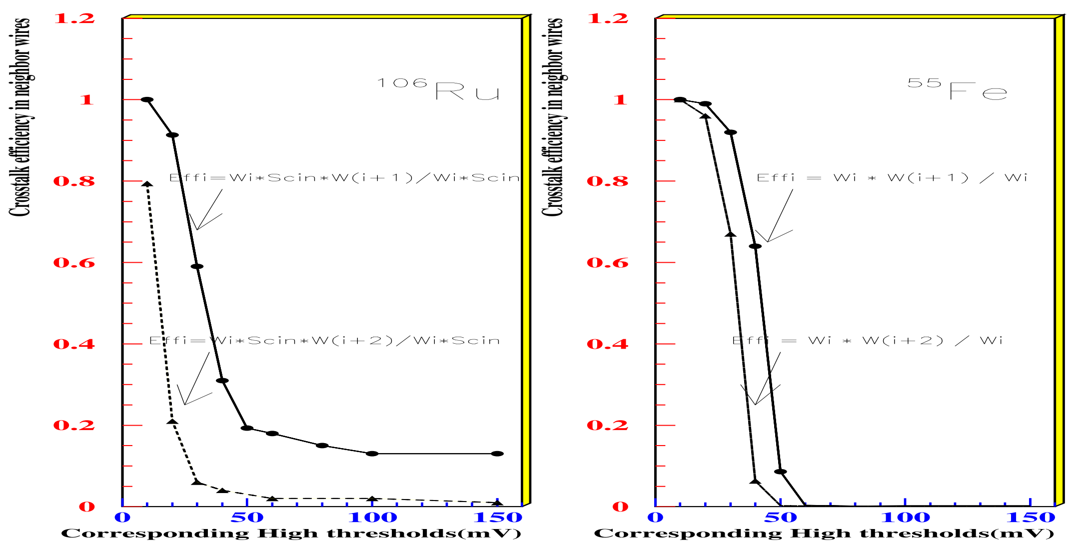

Figure 15: *Cross talk count rates in neighbors vs high thresholds of neighbors. The left one is for ^{106}Ru and the right one is for ^{55}Fe. The curves labeled by the circles correspond to the situation that the tubes lay in the different sublayers of the RSSC, while those labeled by triangles correspond to the situation that the tubes lay in the same sublayer of the RSSC, where 'W$_i$' and 'W$_(i+1)$' represents the hits on tube i and tube (i+1) respectively, and 'Scin' represents the hits on the scintillator.*

position	σ With add-on board (cm)			σ without add-on board (cm)		
z=	W_1	W_2	W_3	W_1	W_2	W_3
40.5 cm	2.33	1.82	2.33	3.88	5.81	4.69
2.0 cm	2.27	1.79	1.91	2.58	2.78	3.09
-40.5 cm	1.91	1.58	1.94	2.67	2.09	2.33

Table 4: *Z resolution comparison for an inner RSSC with/without the add-on board. The ^{106}Ru source was on tube 2 (W_2). The resolutions for W_1, W_2 and W_3 were improved significantly. W_1 indicates tube 1; W_2 indicates tube 2; W_3 indicates tube 3.*

4 Comparative test

Comparative tests with/without the add-on board were done to demonstrate how the new board improves the position resolution.

4.1 Test of an inner RSSC

The first test used an inner RSSC ('S27'). Tube 2 was selected for testing. The test conditions included: 1) the ^{106}Ru source, 2) high voltage 3450 V and 3)Argon/Isobutane: 25%:75%. The tests were done on the downstream and the upstream ends with/without the new electronics, respectively.

Results in Table 4 show that the position resolution improvement was correlated with the source position. A factor of 2 (1.3) improvement was observed on the downstream (upstream) ends.

4.2 Test of an outer RSSC

The same conclusion was obtained from another comparative test of an outer straw chamber 'L40A'. The experimental conditions were similar to those for the smaller inner chamber. The source ^{106}Ru was put on tube 3. Results with/without amplifier are listed in Table 5.

4.3 Selection of the earliest hit tube

In E787, we obtained the z information from the weighted average z of the individual hits in a cluster. In E949, the earliest hit in a cluster is selected as the true hit and its z is used as the z measurement.

Distributions comparison with and without the new electronics is shown in Fig. 16 (Fig. 17) for the inner (outer) RSSC. The right graphs are for the cases without the new electronics[9]. while those on the left are for the cases with the new electronics after the

[9]The threshold was at 10 mV.

position	σ with add-on board(cm)			σ without add-on board(cm)		
z=	W_2	W_3	W_4	W_2	W_3	W_4
37.0 cm	2.67	2.24	2.45	4.09	3.95	3.67
18.5 cm	2.67	1.79	2.49	3.33	3.18	3.58
3.0 cm	2.48	1.61	2.24	3.52	3.03	2.76
-27.5 cm	2.33	1.91	2.06	3.33	3.45	2.46
-46.0 cm	2.24	1.67	2.21	3.09	2.60	2.85

Table 5: *Z resolution comparison for an outer RSSC with/without the add-on board, The ^{106}Ru source was on tube 3 of an outer RSSC. The resolution was improved using the new electronics. W_2 indicates tube 2; W_3 indicates tube 3; W_4 indicates tube 4.*

earliest hit selection[10]. It is evident that the earliest hit selection is helpful further for the resolution improvement and much clean tails can be obtained.

The reason can be given as following. In Fig. 18 shows the relationship between the tube 2 time and the leading edge time[11] difference between tube 2 and its neighbors. It is evident that tube 2 gives better time resolution when it precedes its neighbors. Normally, charged particles hit two tubes simultaneously (one in each sublayer of the RSSC). If the two simultaneously hits arriving within the add-on board coincidence time window[12]. Cross talk from the fast pulse into the other is unavoidable since it superimposes on the signal after which the high threshold is crossed. Thus, averaging the z position from the two simultaneous hits worsens the resolution. The earliest hit in a cluster can be selected to suppress cross talk occurred within the add-on board coincidence time window. 0.2 cm resolution improvement, compared to cases averaging z of the individual hits in a cluster, can be obtained by selecting the earliest hits.

4.4 Tests with production-model electronics

A production-model electronics board with 56 channels was also tested. Two positions on the 'S27A' RSSC were tested on the downstream end (z = 30.25 cm) and the upstream end (z = -38.25 cm). The ^{106}Ru source was moved from tube 1 to tube 12 at each position.

Fig 19 shows the z resolutions with the production board. Run number 1 indicates that the ^{106}Ru source was put on tube 1, and so on. After selecting the earliest hit in a cluster, the typical resolution was about 1.5 cm.

One of the most important issues is the tail of the resolution function. Table 6 shows the tail percentages for cases with the new electronics in two positions. Table 7 shows the tail percentages for cases without the new electronics in different positions. The main peak percentage was counted in a region ±5 cm around the mean position, while "up-tail" means the tail on the left of the main peak and "down-tail" means the tail on the right

[10]The high threshold was at 60 mV and the low threshold was at 10 mV.

[11]In practice, the leading edge times are used as the hit times.

[12]This time window is determined by the high and the low thresholds shown in Fig. 13, approximately 5 ns

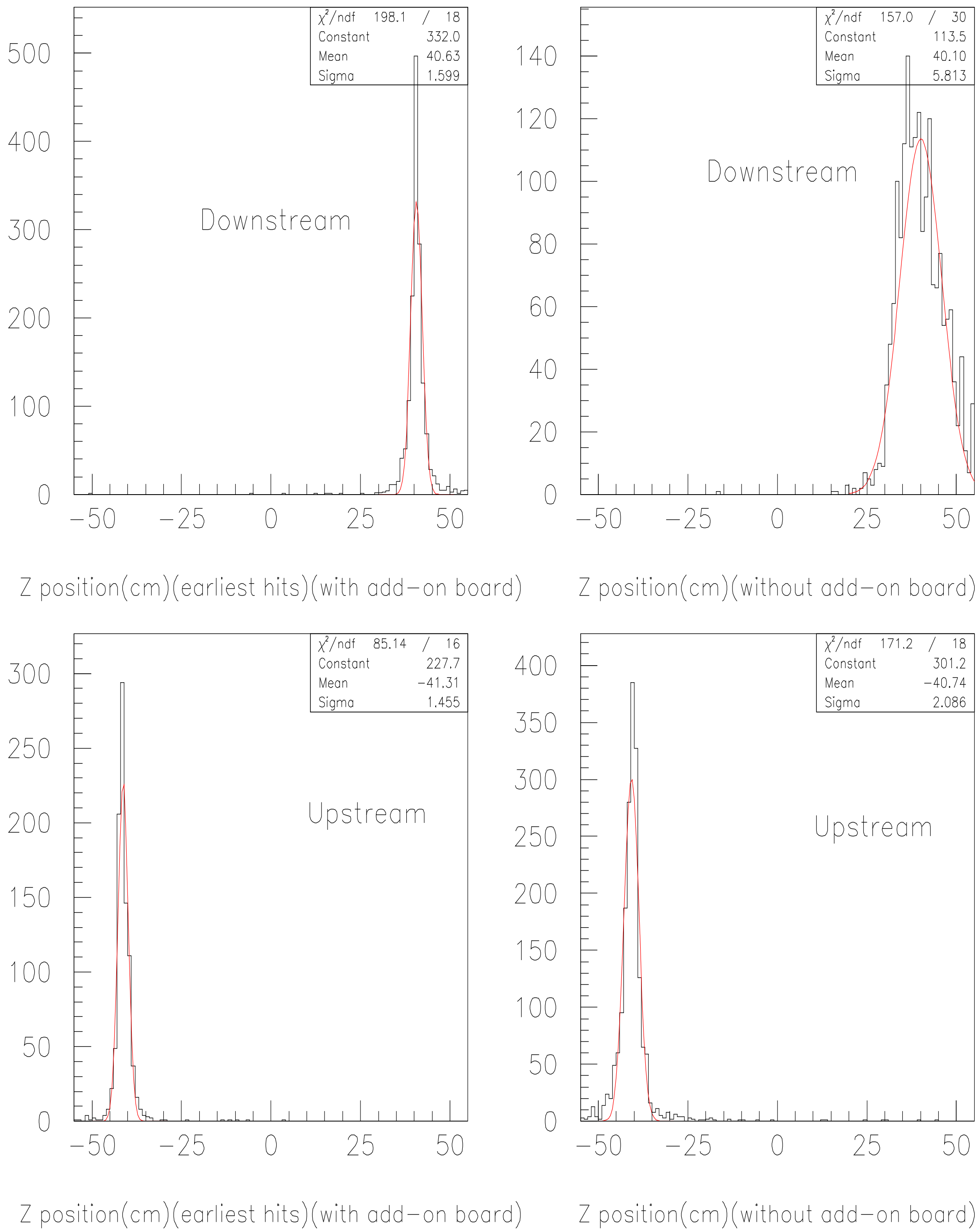

Figure 16: *Z information for an inner RSSC with/without the new electronics. The source ^{106}Ru was on tube 2. Graphs on the left are for cases with the new board (the earliest hit selection was applied), while those on the right are for cases without the new board.*

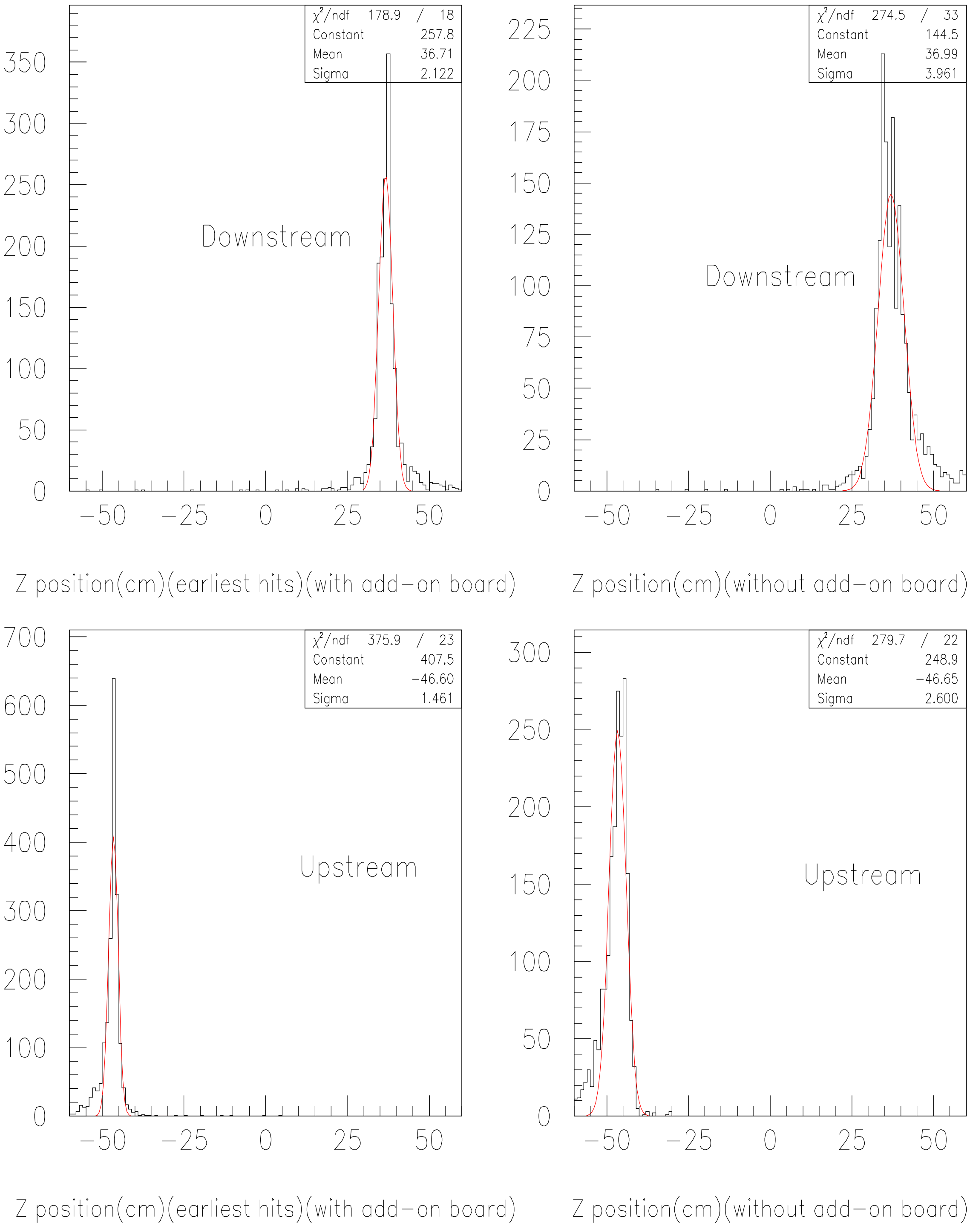

Figure 17: *Z information for an outer RSSC with/without the new electronics. The source* ^{106}Ru *was on tube 3. Graphs on the left are for cases with the new board (the earliest hit selection was applied), while those on the right are for cases without the new board.*

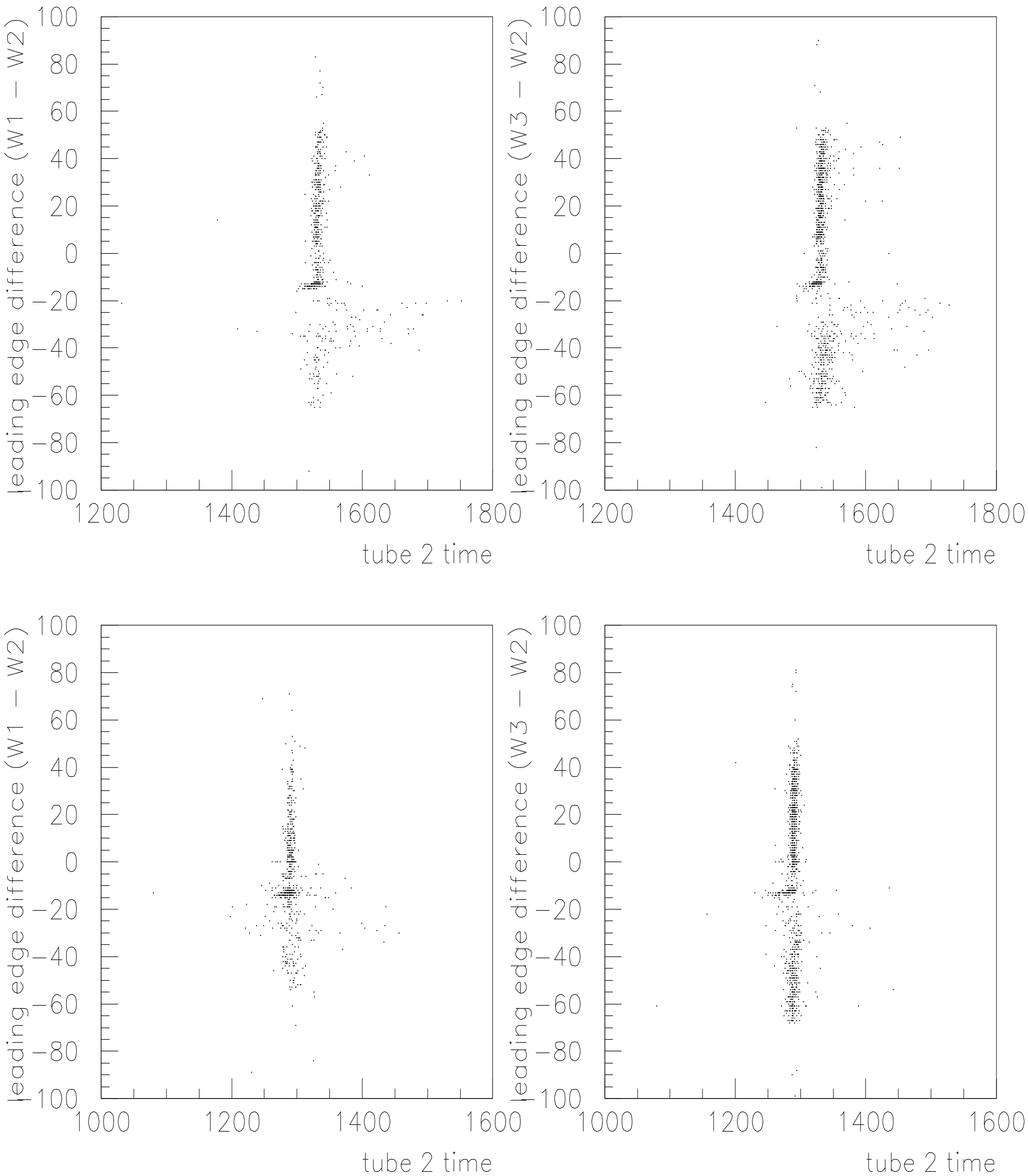

Figure 18: *Leading edge time differences vs tube 2 time. The top row graphs are for the downstream end, while the bottom row graphs are for the upstream end. The left two are for cases related to tube 1 and tube 2; while the right two are for cases related to tube 3 and tube 2. It is evident that tube 2 gives better time resolution when it precedes its neighbors.*

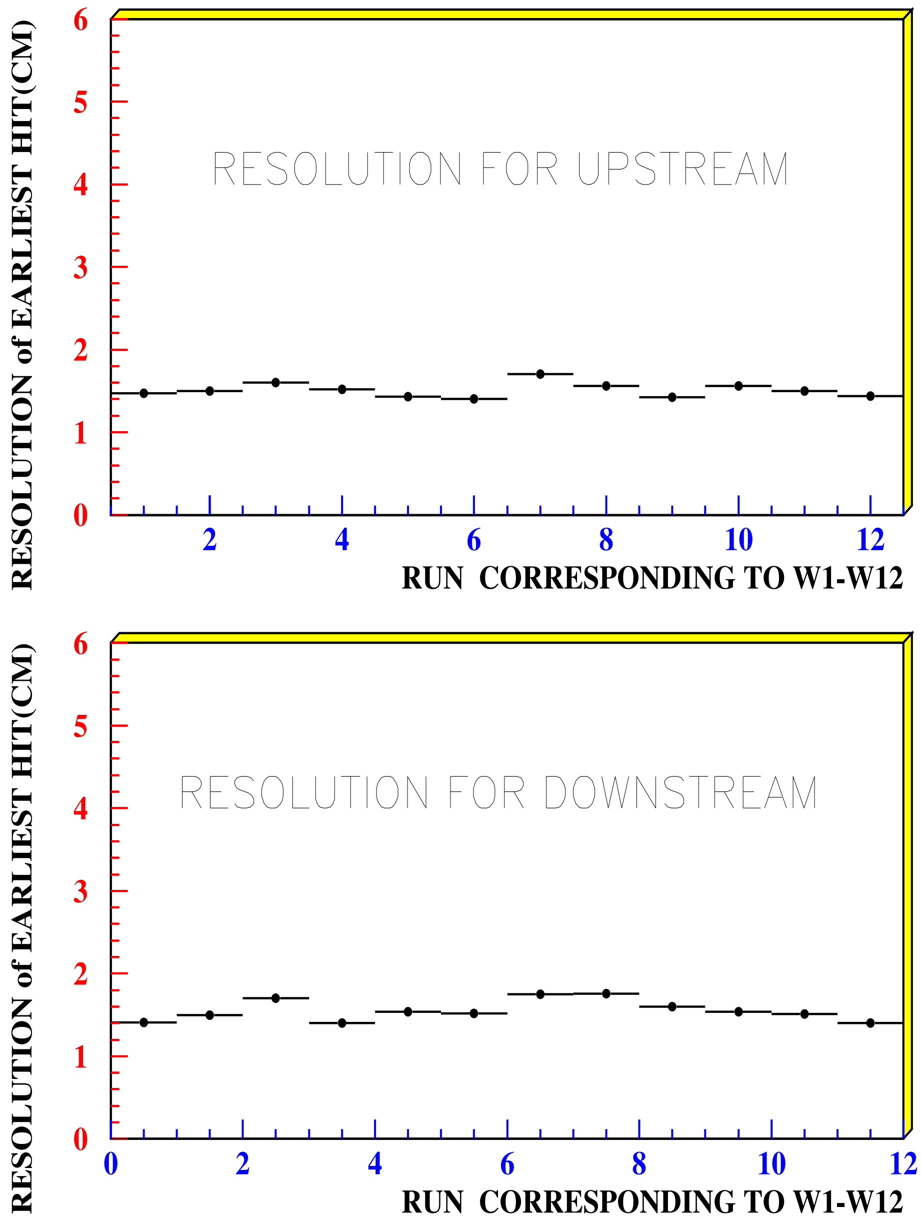

Figure 19: *Z resolution (RMS) vs run/tube number on the upstream and the downstream positions when the new electronics was updated to be able to read 56 channels (earliest hits selection was applied).*

Source	Upstream(%)			Downstream(%)		
W_1-W_{12}	up-tl	main	dw-tl	up-tl	main	dw-tl
W_1	2.59	94.83	2.59	4.35	92.44	3.21
W_2	3.11	94.32	2.57	4.07	92.51	3.42
W_3	3.66	92.49	3.85	4.15	91.93	3.92
W_4	4.17	93.63	2.20	4.10	93.68	2.22
W_5	6.01	91.47	2.52	5.17	90.50	4.54
W_6	3.97	93.28	2.76	4.12	92.93	2.96
W_7	3.24	93.04	3.72	6.95	87.70	5.33
W_8	3.12	93.18	3.65	6.98	89.50	3.53
W_9	3.95	91.69	4.36	4.47	91.36	4.17
W_{10}	1.70	95.65	2.60	1.90	94.15	3.94
W_{11}	3.25	92.47	4.28	2.84	93.30	3.86
W_{12}	2.75	92.23	5.02	4.30	92.22	3.48

Table 6: *Percentages of up-tail (up-tl), main peak and down-tail (dw-tl) in two positions for an RSSC with the new electronics*

position (cm)	up-tl	main	dw-tl (%)
36.5	5.43	87.73	6.84
19.5	5.52	87.15	7.33
-6.5	5.01	88.07	6.92
-32.0	4.93	88.14	6.93

Table 7: *Percentages of up-tail (up-tl), main peak and down-tail (dw-tl) in different positions for an RSSC without the new electronics.*

of the main peak. Compared table 6 with table 7, one can conclude that tails are much cleaner in cases with the new electronics. A typical z distribution with the new electronics is shown in Fig. 20. The tails are only a few percent of the total.

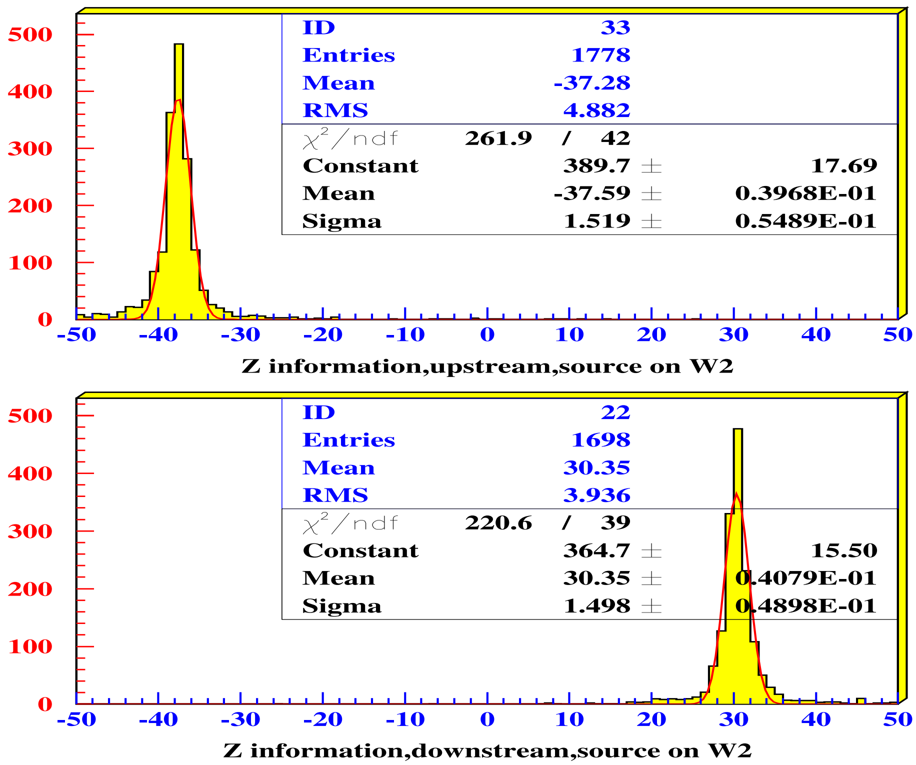

Figure 20: *Position measurements when the source was on tube 2 on the upstream and downstream ends, respectively. The earliest-hit selection was applied.*

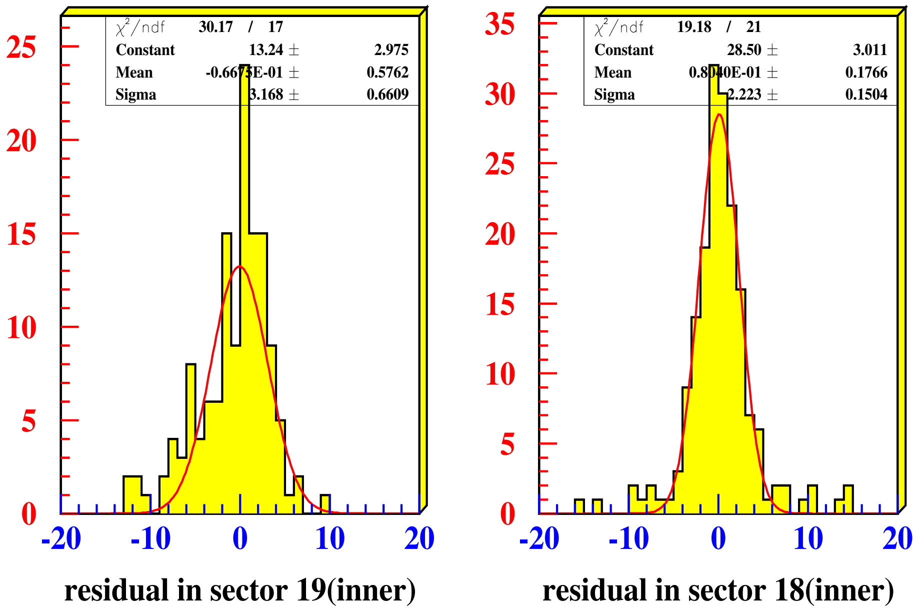

Figure 21: *Cosmic data residual (Z_{utc} - Z_{rssc}) in E949. The graph on the left is from sector 19 without the new electronics, while that on the right is from sector 18 with the new electronics. Better resolution was observed from sector 18.*

5 Results from E949

5.1 Results from cosmic ray data and $K_{\mu 2}$ data

From August 2001 to November 2001, a new electronics board was installed in the sector 18 inner RSSC in E949 to test it's performance. Results from cosmic ray and $K_{\mu 2}$ data showed the consistent z resolution improvement.

High energy cosmic data was used to check the RSSC performance. The results are consistent with the bench tests, as shown in Fig. 21. The resolution of sector 18 is 2.1 cm or 1 cm better than neighboring sectors which have no new electronics[13].

$K^+ \rightarrow \mu^+ \nu_\mu$ data was used to do the same analysis. The results are shown in Fig. 22[14]. After earliest hit selection, sector 18's residual is 1.8 cm and more than one centimeter better than neighbor sectors, which is consistent with the bench test results.

[13] In order to have enough statistics, no earliest selection was used here for the cosmic ray data.

[14] This figure is made after some crucial cuts, such as requiring 6 hits in the UTC r-z planes, good momentum, good individual residuals in the UTC, and good track fitting in order to suppress the uncertainty from the UTC.

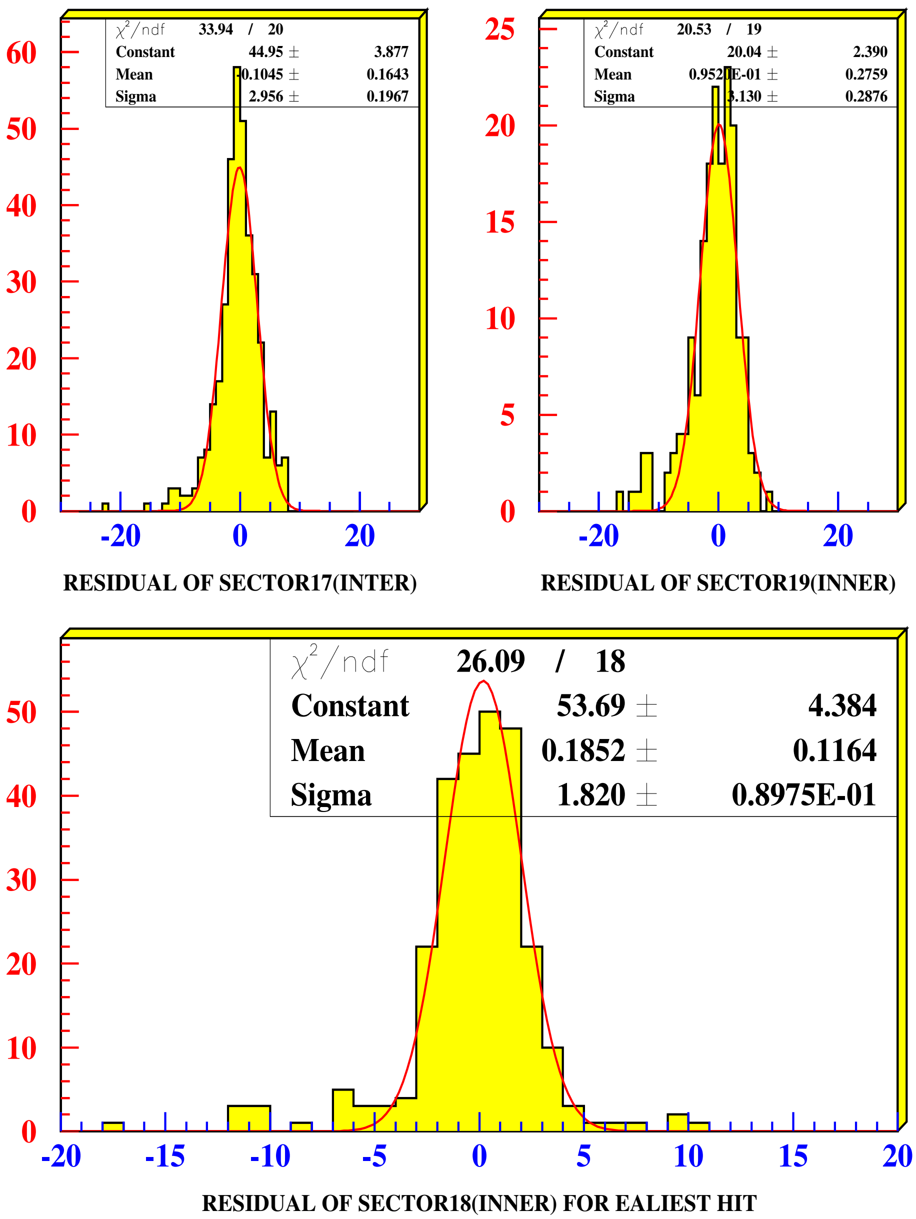

Figure 22: *Residuals of (Z_{UTC} - Z_{RSSC}) in sectors 17,18 and 19 in E949. The resolution in sector 18 is 1 cm better than neighbors.*

	2002 data		1998 data	
	$K_{\mu 2}$	π_{scat}	$K_{\mu 2}$	π_{scat}
Inner	94.5±1.6	97.4±1.5	99.1±0.08	99.0±0.2
Outer	97.3±1.4	98.1±1.5	99.6±0.07	99.6±0.3

Table 8: *The Efficiency comparison for the 2002 and 1998 data.*

5.2 Efficiency

The RSSC efficiencies were obtained using RS counters in the same sector as trigger which are located at the inside and outside of the RSSC, i.e., requiring the charged track passing through both layers inside and outside of the RSSC, and checking if the RSSC fired or not. For an inner RSSC, the efficiency is defined as "(layer10 · RSSC · layer11)/(layer10 · layer11)" and for an outer RSSC, it is defined as "(layer14 · RSSC · layer15)/(layer14 · layer15)".

The E949 RSSC efficiencies were measured using the $K_{\mu 2}$ and the π_{scat} data. The average efficiencies for working RSSCs[15] are shown in table 8. The efficiency losses in the $K_{\mu 2}$ data, compared to the 98 data, can be explained as following. The energy losses from muons in the RSSCs are lower than those from pions due to the smaller mass. Thus, the smaller signal amplitudes of muons could lead to the signals from the trailing edge tubes missing if the current high thresholds are high enough to cut some of them. The worse $K_{\mu 2}$ efficiencies in the inner RSSCs also illustrate that the signal amplitudes have an impact on the efficiency losses since muons have smaller energy losses in the inner RSSCs due to the relatively larger traversing velocity. The estimated efficiency errors are much bigger than those in 1998 due to the lower statistics available at present[16].

6 Conclusion

This report describes an improvement to the RSSC electronics system which results in improved performance. New electronics was designed to be added between the chamber and the coincidence board, which uses two discriminators. This modification reduces time walk using a low threshold discriminator and suppresses cross talk using a high threshold discriminator. Z resolution about 1.5 cm was achieved in bench tests. In E949, the results from $K_{\mu 2}$ data and cosmic data showed consistent z measurement improvements.

[15] Ignoring those RSSCs which can not work well, including sector 9 inner RSSC and sector 7 outer RSSC.

[16] The error is estimated by the following formula:

$$Error = \sqrt{\frac{P(1-P)}{N}} \tag{9}$$

where P is the efficiency and N is the denominator when doing the efficiency calculation.

References

[1] Frank E.Taylor, Nuclear Instruments and Methods A289(1990)

[2] G. Charpak et al., IEEE Trans. Nucl. Sci. NS-25 (1978) 122.

[3] J. Fisher, Nucl. Instr. and. Meth. 151 (1978) 451.

[4] M. Atac and A.V. Tollestrup, Preprint FN-339, Fermilab (July 10, 1981).

[5] D. Potter, Nuclear Instr and Meth 200 (1982) 345-354

[6] V.A. Lozanskii and O.B.Firsov, Sov.Phys. JETP 29 (1969) 267.

[7] E. Iarocci, Nucl. Instr. and. Meth. 217 (1983) 30-42.

[8] G. Battistoni, E. Iarocci, Nucl. Instr. and. Meth. 164 (1979) 57-66.

[9] Robert A.McPherson, Ph.D thesis, Princton University (1995)